Hyodo et al. Earth, Planets and Space (2016) 68:6
DOI 10.1186/s40623-016-0384-6

Earth, Planets and Space
a SpringerOpen Journal

FULL PAPER Open Access

A possible scenario for earlier occurrence of the next Nankai earthquake due to triggering by an earthquake at Hyuga-nada, off southwest Japan

Mamoru Hyodo[1*], Takane Hori[1] and Yoshiyuki Kaneda[2]

Abstract

Several recent large-scale earthquakes including the 2011 Tohoku earthquake (M_w 9.0) in northeastern Japan and the 2014 Iquique earthquake (M_w 8.1) in northern Chile were associated with foreshock activities ($M_w > 6$). The detailed mechanisms between these large earthquakes and the preceding smaller earthquakes are still unknown; however, to plan for disaster mitigation against the anticipated great Nankai Trough earthquakes, in this study, possible scenarios after M_w 7-class earthquakes that frequently occur near the focal region of the Nankai Trough are examined through quasi-dynamic modeling of seismic cycles. By assuming that simulated Nankai Trough earthquakes recur as two alternative earthquakes with variations in magnitudes (M_w 8.7–8.4) and recurrence intervals (178–143 years), we systematically examine the effect of the occurrence timing of the M_w 7 Hyuga-nada earthquake on the western extension of the source region of Nankai Trough earthquakes on the assumed Nankai Trough seismic cycles. We find that in the latter half of a seismic cycle preceding a large Nankai Trough earthquake, an immature Nankai earthquake tends to be triggered within several years after the occurrence of a Hyuga-nada earthquake, then Tokai (Tonankai) earthquakes occur with maximum time lags of several years. The combined magnitudes of the triggered Nankai and subsequent Tokai (Tonankai) earthquakes become gradually larger with later occurrence of the Hyuga-nada earthquake, while the rupture timings between the Nankai and Tokai (Tonankai) earthquakes become smaller. The triggered occurrence of an immature Nankai Trough earthquake could delay the expected larger Nankai Trough earthquake to the next seismic cycle. Our results indicate that triggering can explain the variety and complexity of historical Nankai Trough earthquakes. Moreover, for the next anticipated event, countermeasures should include the possibility of a triggered occurrence of a Nankai Trough earthquake by an M_w 7 Hyuga-nada earthquake.

Keywords: Nankai Trough earthquake, Hyuga-nada earthquake, Triggered scenario

Introduction

It is well known from historical seismology that M_w 8 earthquakes have been recurring at the Nankai Trough since 684 CE, causing severe damage to the Japanese Islands. As shown in Fig. 1, approximately nine successive Nankai Trough earthquakes (in 1946 and 1944, 1854, 1707, 1605, 1498, 1361, 1099 and 1096, 887, and 684) have been documented in the historical record over the past 1300 years (Ishibashi 2004). As summarized in Ishibashi (2004), occurrences of these historical Nankai Trough earthquakes have been found in historical documents around Kyoto, the Japanese capital from the end of the eighth century to the beginning of the seventeenth century. Since the region around Kyoto is strongly impacted by not only the Nankai Trough earthquakes but also by nearby inland earthquakes, the occurrences of historical Nankai Trough earthquakes have been chosen by carefully compiling reliable historical descriptions or records that detail the typical interplate event along the

* Correspondence: hyodo@jamstec.go.jp
[1]Research and Development Center for Earthquake and Tsunami, Japan Agency for Marine-Earth Science and Technology, Yokohama 236-0001, Japan
Full list of author information is available at the end of the article

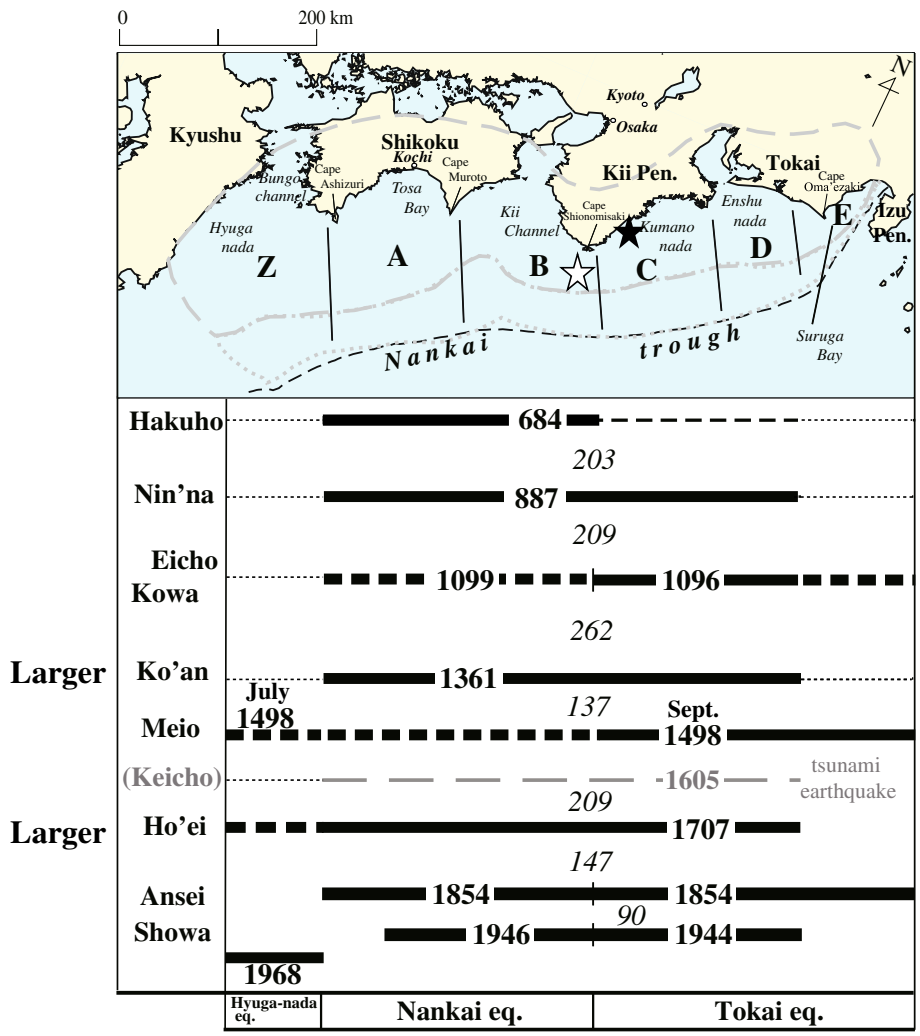

Fig. 1 Historical sequence of Nankai Trough earthquakes (after Ishibashi 2004). *Upper map* shows distribution of six rupture segments along Nankai Trough. Each rupture segment has been broken or unbroken in historical Nankai Trough earthquakes. Areas surrounded by *gray dashed* and *gray dotted lines* represent maximum estimates of seismogenic sources and possible tsunamigenic sources for future Nankai Trough earthquakes, respectively (Cabinet Office 2012). *Black* and *white stars* indicate hypocenters of the 1944 Tonankai and 1946 Nankai earthquakes, respectively (Kanamori 1972). In the table below, *horizontal thick lines* indicate segments that ruptured during each historical event in the Japanese eras named in the *left column*. *Thick dashed lines* and *thin dotted lines* indicate probable and possible broken segments, respectively. *Roman* and *italic numerals* indicate earthquake occurrence years and time intervals between two successive earthquakes, respectively. Since the 1605 Keicho event (shown by a *gray broken line*) was obviously a tsunami earthquake, this event is excluded in counting the time intervals between successive events. Among successive earthquakes, the 1707 Ho'ei and 1361 Ko'an earthquakes are considered to be larger earthquakes than ordinary ones from the evidences of uplifts and large tsunamis at the southern tip of the Kii Peninsula (e.g., Shishikura et al. 2011)

Nankai Trough; these include strong ground motion, felt aftershocks in Kyoto, large tsunami damages along the Pacific coast, coseismic vertical deformation at coastal regions (uplift of the capes Muroto and Oma'ezaki, subsidence of the Kochi plain), and temporal inactivities of specific hot springs. By comparing the timing of a possible Nankai Trough earthquake with contemporary geological evidences of the occurrence of strong shaking (traces of liquefaction at ruins) or large tsunamis (tsunami deposits in coastal lakes), the reliability of the possible Nankai Trough events has been checked from another viewpoint (e.g., Sangawa 2009; Shishikura et al. 2011). These contemporary geological evidences especially help historical seismologists constrain the spatial extent or magnitude of the historical Nankai Trough earthquakes. In Fig. 1, the horizontal thick black solid lines denote certain rupture segments in historical Nankai Trough earthquakes. Judging from the completeness of reliable historical materials, thick and thin black broken lines are probable and possible rupture segments in historical Nankai Trough earthquakes, respectively. The thin dotted lines denote unknown rupture segments during the historical

Nankai Trough earthquakes. White blanks indicate seismic gaps. The gray broken line in 1605 denotes a tsunami earthquake with no evidence of severe seismic hazard. As shown in Fig. 1, a recurrence interval between the 1099 Kowa Nankai earthquake and 1361 Ko'an Nankai Trough earthquake is 262 years, which is almost twice as long as the average interval after the 1361 Nankai earthquakes. Therefore, historical seismologists consider there may be a hidden Nankai Trough earthquake during this period. However, a new reliable earthquake around the thirteenth century has not been confirmed from historical materials yet there exist contemporary traces of liquefaction that are not inconsistent with the damages of the Nankai Trough earthquake in Osaka and the southern tip of the Kii peninsula (Sangawa 2011).

For the current sequence of reliable Nankai Trough earthquakes, there have been large variations in the magnitudes (M_w = 8.0–8.7) and recurrence intervals (90–262 years) of successive Nankai Trough earthquakes, with different rupture extents along the Nankai Trough. Additionally, in some successive earthquakes, the eastern and western segments of the Nankai Trough have ruptured separately, with large variations in time lags: about 3 years between the 1099 and 1096 events, 2 years between 1946 and 1944, several days for the 1361 events, and 30 h in the 1854 events. In most of the events with such rupture separation, the eastern segment ruptured first, followed by the western segment. For the recent 1946 and 1944 Nankai Trough earthquakes, which were observed by modern observation instruments such as seismograms and tide gauges, the hypocenter locations were estimated from the observed data (Kanamori 1972): the 1944 Tonankai earthquake initiated at Kumano-nada, on the eastern side of the Kii Peninsula, while the 1946 Nankaido earthquake initiated in the eastern part of the Kii channel, on the western side of the southern tip of the Kii Peninsula (see solid and open stars in Fig. 1). Only for the 1498 Meio event is there a possibility that rupture on the western segment preceded that on the eastern segment, based on combined interpretation of Japanese and Chinese historical documents (Tsuji 1999).

The recent successive earthquakes in 1946 and 1944 were the smallest events among the historical Nankai Trough events. Seventy years have passed since those events, approaching the minimum recurrence interval (90 years between the 1944 and 1854 events) between successive Nankai Trough earthquakes. Accordingly, the application of the time-predictable model (Shimazaki and Nakata 1980) to the recent Nankai Trough earthquake sequence predicts a short recurrence interval to the next earthquake, considering the small magnitudes of the 1946 and 1944 events. Hence, the occurrence of the next Nankai Trough earthquake has been anticipated for several decades (Headquarters for Earthquake Research Promotion 2001).

Recently, the M_w 9 Tohoku earthquake occurred unexpectedly in 2011 and generated a very large tsunami. Following this unexpected great earthquake, the damage expectation and the occurrence probability for the next Nankai Trough earthquake have been revised by government agencies (e.g., Cabinet Office 2012; Headquarters for Earthquake Research Promotion 2013). However, the published damage expectation was based on a kinematic model for a much larger earthquake scenario ($M_w \sim 9$) than the historical earthquakes ($M_w \sim 8$). It is not necessary that the damage expectation due to kinematic scenarios of M_w 9 earthquakes is greater than the damages due to possible M_w 8 earthquakes with various rupture patterns, and the damage estimate based only on one large M_w 9 earthquake might be inadequate. Therefore, it is indispensable to examine not only an M_w 9 scenario but also various possible M_w 8 scenarios.

Many complex physical processes that contribute to earthquake generation, such as fault friction and fault interactions, are not well known. Although we cannot model all of the processes, we should examine the possible and more physically plausible scenarios predicted by various models. Recently, numerical simulations of earthquake occurrences, than those obtained via kinematic earthquake models, have been executed for the purpose of obtaining various earthquake scenarios that are more physically plausible, assuming a fault constitutive law and fully elastodynamic interactions during earthquake ruptures (e.g., Hok et al. 2011; Noda and Lapusta 2013). In Japan, for interpreting previous seismic cycles and examining possible future scenarios, quasi-dynamic seismic cycle simulations have been widely conducted based on the rate- and state-dependent friction law and quasi-static slip response functions. For the Japan Trench in the northeastern part of Japan Islands, quasi-dynamic earthquake cycle modeling with rate- and state-dependent friction and stress accumulation due to the subducting Pacific plate have been implemented, with the aim of examining possible seismic cycles including multi-scale asperities with the patch size of 10^0–10^2 km (e.g., Shibazaki et al. 2011; Kato and Yoshida 2011; Ohtani et al. 2014; Ariyoshi et al. 2014). Additionally, along the Nankai Trough, similar quasi-dynamic seismic cycle simulations of M_w 8-class earthquakes due to the subduction of the Philippine Sea plate have been conducted (e.g., Hori et al. 2004; Hori 2006). Moreover, aseismic events recently observed in the Nankai Trough region have also been successfully modeled in the framework of quasi-dynamic earthquake cycle model. Long-term slow slip event (SSE) beneath Tokai, eastern part of the Nankai trough region, was reproduced with M_w 8-class Nankai Trough earthquakes (Hirose and Maeda 2013). As for the western side of the Nankai

Trough, Shibazaki et al. (2010) and Matsuzawa et al. (2010) modeled SSEs, occurring in the deeper part of the seismogenic zone of the M_w 8-class earthquake beneath Shikoku, by using a modified version of the rate- and state-dependent friction laws. Subsequently, it has been discussed that the stress buildup process in an M_w 8 earthquake cycle affects the recurrence behavior of SSEs (Matsuzawa et al. 2010; Ariyoshi et al. 2012)

In order to deduce the possible mechanism for the variation in magnitude and recurrence intervals in the three recent Nankai Trough seismic cycles (1944–1946, 1854, and 1707), Hori (2006) modeled the three seismic cycles by focusing on the relationship between the variation of recurrence intervals and the time gaps between the ruptures of the Tokai (eastern) and Nankai (western) earthquakes. Thus, by assuming frictional heterogeneity beneath the Kii Peninsula, which behaves as a barrier to rupture propagation, he found that Nankai Trough earthquakes tend to initiate off Kumano-nada, where the oceanic plate is subducting at a steep dip angle, and the increase in time intervals between rupture on the eastern and western segments with seismic cycles (from concurrent rupture to several years of time lag) occurs simultaneously with shortening of the recurrence intervals (111–95 years). Although a quantitative comparison of the recurrence intervals shows large gaps between simulated and historical values, this is qualitatively consistent with the increasing time intervals between rupture on the eastern and western segments in the three recent seismic cycles (e.g., simultaneous in 1707, 30 h in 1854, and 2 years in 1944 and 1946) and the shortening of the recurrence intervals (209, 147, and 90 years). Furthermore, Hori et al. (2009) suggested that seismic cycle simulations with nesting asperities (hierarchical asperity) with different fracture energies explained much larger variation of earthquake magnitudes and recurrence intervals because of the remarkable change in the stressing rate near the earthquake nucleation point (off Kumano-nada for Nankai Trough earthquakes) between seismic cycles. By applying the hierarchical asperity model to the Nankai Trough seismic cycles, Hyodo and Hori (2013) reproduced the large variations in magnitude (M_w = 8.58–8.97) and recurrence intervals (168–204 years) for the Nankai Trough earthquakes. The difference in the recurrence intervals is consistent with that of the historical sequence, except for the short recurrences of the Showa events. As mentioned above, some characteristics of the Nankai Trough earthquake sequence have been explained as variations of the seismic cycles. Thus, these quasi-quantitative reproductions of previous patterns of Nankai Trough earthquakes suggest that we can use such earthquake cycle models to examine possible Nankai Trough earthquake scenarios.

Recently, through similar numerical simulations of interplate seismic cycles along only the western half of the Nankai Trough from Kyushu to Shikoku, Nakata et al. (2014) found that there exists a possible earthquake scenario in which the Nankai earthquake rarely initiates off the western edge of Shikoku Island about 5 years after the occurrence of the Hyuga-nada earthquake, although most Nankai and Hyuga-nada earthquakes occur independently, and most Nankai earthquakes initiate at the Kii Peninsula, on the eastern edge of their model region. Since such a rare Nankai earthquake is triggered by a Hyuga-nada earthquake, the recurrence interval from the previous Nankai earthquake is considerably shortened, thus its magnitude is smaller than those with non-triggered ruptures. M_w 7 Hyuga-nada earthquakes have historically occurred at the western extension of the source area of Nankai Trough earthquakes, and in the 1498 Meio event, one of the Hyuga-nada earthquakes may have enhanced the initiation of the Nankai earthquake at the western edge of Shikoku Island. Hence, we propose to evaluate the possible effect of realistic conditions with an M_w 7-class asperity for the entire Nankai Trough, including the eastern segments.

In this paper, by extending the seismic cycle model of Nakata et al. (2014) toward the eastern part of the Kii Peninsula, we first examine the conditions under which the westward triggering of Nankai earthquakes occurs. Then, we systematically examine the possible effect of trigger timing on the recurrence intervals of Nankai Trough earthquakes and rupture timing between the eastern and western segments. Finally, we discuss the possibility of the triggered Nankai Trough earthquake scenario as the next earthquake.

Methods

In order to confirm the effect of the interaction between Nankai Trough earthquakes and Hyuga-nada earthquakes on the entire Nankai Trough earthquake cycle, with a model plate interface extending from Kyushu to the Tokai area, we use the same numerical simulation procedure of Nakata et al. (2014). The seismic cycle calculation is described as a coupling of the quasi-dynamic expression of fault stress and rate- and state-dependent fault friction. The governing equations are as follows:

$$\tau(\mathrm{x},t) = \int_{\Omega} G(\mathrm{x}:\mathrm{x}_0)\left(u(\mathrm{x}_0,t) - V_p(\mathrm{x}_0)t\right)dx_0 - \eta V(\mathrm{x},t) \tag{1}$$

$$V = V_* \exp\left[\frac{\tau - \left(\tau_s^* + \Delta\tau_s\right)}{A}\right] \tag{2}$$

$$\frac{d\Delta\tau_s}{dt} = \frac{B}{L/V_*}\exp\left(-\frac{\Delta\tau_s}{B}\right)\exp\left(-\frac{V}{V_c}\right) - \frac{V}{L}\left\{\Delta\tau_s + B\ln\left(\frac{V}{V_*}\right)\right\}. \quad (3)$$

Equation 1 is an approximated expression of fault shear stress τ in the subduction direction using the static slip response to unit forward slip G, slip deficit on the plate interface $V_p t - u$, and fault slip rate V. The first term on the right-hand side of this equation represents a quasi-static fault shear stress as the spatial integration of the product of G and slip deficit over the target plate interface Ω, where u and V_p are the slip and prescribed back-slip rate on the plate interface, respectively. V and u have the relation of $du/dt = V$. The second term represents the effect of radiation damping introduced by Rice (1993), the coefficient η controls the degree of the effect of the seismic radiation, and $\eta = \mu/2\beta$ is assumed following Rice (1993), where μ and β are the rigidity and shear wave velocity of the material surrounding the source region, respectively. In the following, we set $\mu = 30$ GPa and $\beta = 3.27$ km/s.

Equation 2 represents a rate- and state-dependent friction, where V_*, τ_s^*, and $\Delta\tau_s$ are an arbitrary reference slip velocity on the frictional surface, the strength of a fault sliding with a velocity of V_*, and the differential fault strength measured from τ_s^*, respectively. Because Eq. 2 implies the slip rate V is accelerated or decelerated from V_* depending on the difference between the fault shear stress τ and the variable τ_s ($=\tau_s^* + \Delta\tau_s$), the variable τ_s is regarded as a threshold to acceleration of the fault with respect to the fault shear stress τ. Hence, we call the variable τ_s as the "strength" of the fault. A frictional parameter A ($=a\sigma$) controls the variation of V with respect to the certain difference of stress and strength, where parameter a (and b, as will be described below) is a frictional coefficient, and σ is the effective normal stress. The differential strength $\Delta\tau_s$ here is defined as $\Delta\tau_s = B\ln(V_*\theta/L)$, where θ is the state variable representing a contact state of the interface and B ($=b\sigma$) and L are also frictional parameters controlling strength recovery and slip weakening. It should be noted that we can obtain the ordinary rate- and state-dependent friction equation by substituting the definition of $\Delta\tau_s$ in Eq. 2. Equation 3 is an equivalent differential equation to the composite equation describing the evolution of the state variable θ (Kato and Tullis 2001), although the integrand is $\Delta\tau_s$ instead of θ. The composite equation deduced by Kato and Tullis (2001) was made by slightly modifying existing rate- and state-dependent friction laws (slip law and slowness law) originally developed by Dieterich (1979) and Ruina (1983) so that a wide range of experimental observations are fitted. The first term on the right-hand side of Eq. 3 expresses the time-dependent increase of $\Delta\tau_s$ (healing effect) if the slip rate V is small enough ($V \sim V_c$), while the second term represents the slip-dependent decrease of $\Delta\tau_s$ (slip-weakening effect). Thus, V_c switches the behavior of Eq. 3, depending on the slip rate V, and is called the cutoff velocity. Following Kato and Tullis (2001), we assume $V_c = 10^{-8}$ m/s in Eq. 3 to fit the theoretical frictional property to the experimental data of friction on granite surfaces obtained by Blanpied et al. (1998). For $V >> V_c$, the steady-state shear stress τ^{ss} is defined for $d\Delta\tau_s/dt = 0$, and $\tau^{ss} = \tau_s^* + (A - B)\ln(V/V_*)$. When $A - B < 0$, the steady-state stress decreases with an increase in slip velocity (velocity weakening), possibly leading to unstable slip (earthquake). In the case of $A - B > 0$, stress increase with slip velocity (velocity strengthening) and steady slip or aseismic slip can occur. Accordingly, A ($=a\sigma$), B ($=b\sigma$), and L in Eqs. 2 and 3 largely affect the seismic cycles on the plate interface. Though A ($=a\sigma$) and B ($=b\sigma$) depend on the normal stress σ which could vary with seismic cycles, we neglect the temporal variation of σ for simplification.

Note that we abbreviate the functional expressions as variables in Eqs. 2 and 3: the variables V_*, τ_{*s}, A, B, and L are functions with respect to only the spatial coordinate (i.e., constant in time), while V_c ($=10^{-8}$ m/s) is constant with respect to time and space. V, τ, and $\Delta\tau_s$ are unknown variables with respect to time and space.

By spatially discretizing the governing equations above, the target plate interface Ω is divided into a set of N small finite sub-faults. Then, simultaneous differential equations with respect to slip rate V_i and differential fault strength $\Delta\tau_{s,i}$ are deduced, where the subscript i indicates an index for the sub-faults ($1 < i < N$). The differential equation with respect to $\Delta\tau_{s,i}$ is directly obtained from Eq. 3, and it is obvious that the evaluation of $d\Delta\tau_{s,i}/dt$ on each sub-fault i can be executed by using the variables on its own sub-fault only. Meanwhile, the concrete expression of the evolution of slip rate V_i is deduced from Eqs. 1 and 2 as follows:

$$\frac{dV_i}{dt} = \frac{V_i}{A_i(1 + \eta V_i/A_i)}\left\{\sum_{j=1}^{N} G_{ij}\left(V_j - V_{p,j}\right) - \frac{d\Delta\tau_{s,i}}{dt}\right\}. \quad (4)$$

Here, subscripts i and j indicate indexes for the sub-faults ($1 < i,\ j < N$). Thus, it should be noted that the direct evaluation of dV_i/dt for all i requires $O(N^2)$ operation, since G_{ij}, which is the slip response on sub-fault i due to unit slip on sub-fault j, becomes an $N \times N$ dense matrix. Hence, in the quasi-dynamic earthquake cycle simulation with a large sub-fault number N, direct evaluation of Eq. 4 requires a large memory for G_{ij}, and it becomes the most time-consuming process.

For efficient calculation of seismic cycles, many attempts to reduce memory sizes and computation time

associated with Eq. 4 have been examined (Kato 2008; Tullis et al. 1999; Ohtani et al. 2011; etc.). Among these, we adopted the procedure used in Ohtani et al. (2011), which applied the method of hierarchical matrices (H-matrices) to multiplicative computations of $N \times N$ slip response function matrix and the slip deficit rate vector. In contrast to other attempts, the quasi-dynamic simulation using H-matrices is easily applicable to a seismic cycle on a 3-D curved interface, since H-matrices are just mathematical approximations as low-rank compressed representations of the original dense matrix G_{ij}. Thus, independent of the target fault configuration or earthquake slip direction, H-matrix approximation is applicable to quasi-dynamic cycle simulations and is suitable to our target problem. Following Ohtani et al. (2011), the original computation time of arithmetic operation with $O(N^2)$ will be efficiently reduced to $O(N \log N)$ for N which we treat here (10^5–10^6), while memory size will be reduced to about $O(N)$.

For more efficient computation of seismic cycles, we execute simulations with H-matrices on massively parallel computers. In the parallelized simulation code, the total sub-faults are divided into groups depending on the number of usable CPUs. Then, the velocities V_i and differential strengths $\Delta\tau_{s,i}$ in each group are assigned on a CPU in charge of each group. Also, the CPU stores only a subset of H-matrices that are used for the evaluation of velocity rates dV_i/dt on each group. Though each CPU contains only velocities of a group in charge of each CPU, current velocities on all sub-faults are necessary for evaluating Eq. 4. Hence, before evaluating Eq. 4 on each CPU, velocities on all sub-faults are collected through the message passing interface (MPI) communication; then, the evaluations of Eq. 4 are calculated on each CPU. Calculated slip velocity rates and strength rates are used for the time integration by the adaptive-stepping fifth-order Runge-Kutta method (Press et al. 1996).

As shown in Fig. 2, we model the plate interface between the overlying continental plate and the subducting Philippine Sea plate along the Nankai and Suruga Troughs, from southern Kyushu to Suruga Bay. Here, similar to Nakata et al. (2014), a discretized 3-D Philippine Sea plate interface geometry of Baba et al. (2002) is adopted, because the purpose of this study is motivated by a possible model in Nakata et al. (2014). The interface geometry of the seismogenic zone in Baba et al. (2002) is based on seismic surveys, because the low interplate seismicity along the Nankai trough makes it difficult to draw the interface geometry from the location of interplate earthquakes. Hence, the use of Baba et al. (2002) is suitable to our modeling mainly concerning large earthquakes in the seismogenic zone. However, in Baba et al. (2002), the geometry at the shallowest part of the interface is extrapolated from the geometry at the reliable seismogenic depth, and we consider the depth range of the interface from 6 to 45 km in the vertical direction. Then, to divide the plate interface of Baba et al. (2002) into sub-faults, we define a 3-D coordinate system, as shown in Fig. 2a. Using this coordinate system, the plate interface is divided into sub-faults so that the projections of sub-faults onto the Y-Z plane form homogeneous rectangular grid cells (see Fig. 3a). For these sub-faults, we prepare the slip response G_{ij} in Eq. 4 as the stress change enhances the slip of the sub-fault i due to unit slip of sub-fault j. Since sub-faults generally form non-planar configurations, we approximate a sub-fault with a set of three triangles, as shown in Fig. 3b. Then, G_{ij} is evaluated at the center of the sub-fault i (crosses in Fig. 3b) as the combined stress change due to unit slips on a set of three triangles representing sub-fault j. The direction of a unit slip on each triangle in a sub-fault is determined from the direction of subduction and the configuration of the triangle (i.e., strike and dip) as follows. First, we divide the horizontal unit vector with the direction of subduction direction into two components: the strike direction of the triangle and the direction perpendicular to it. Then, the latter component of the unit vector is rotated to the direction of the dip of this triangle, and this rotated vector is assumed to become the dip component of the unit slip. Finally, we define the tangential slip which can occur on the triangle as the dislocation along the unit vector consisting of the strike and dip components as mentioned above.

By setting $\Delta Y = 1$ km and $\Delta Z = 0.1$ km, as in Fig. 3a, and discretizing the model plate interface into sub-faults less than 1 km^2 in size, the total number of sub-faults treated here is 308,736. For these discretized sub-faults, the set of slip responses G_{ij} in Eq. 4 is evaluated in a homogeneous elastic half space, and they are compressed as H-matrices as mentioned above. Then, the vertical position of the free surface of the elastic half space is set at 5 km depth of the interface geometry of Baba et al. (2002). This means that the upper limit of the model interface does not reach the seafloor (i.e., free surface). When it reaches the seafloor, the shallow slip becomes too large, and the rupture becomes difficult to stop, as shown in Hyodo and Hori (2013).

We project the same distribution of A, B, L, and V_p as in Nakata et al. (2014) onto the plate interface from Kyushu to Shikoku; then, for the frictional parameters A, B, and L, we extrapolate the depth profiles for eastern Shikoku further along the eastern plate interface (Fig. 2b, c). For back-slip rate V_p, the direction is assumed to be N 55° W similar to Nakata et al. (2014). In size of back-slip rate, a gradual decrease is assumed

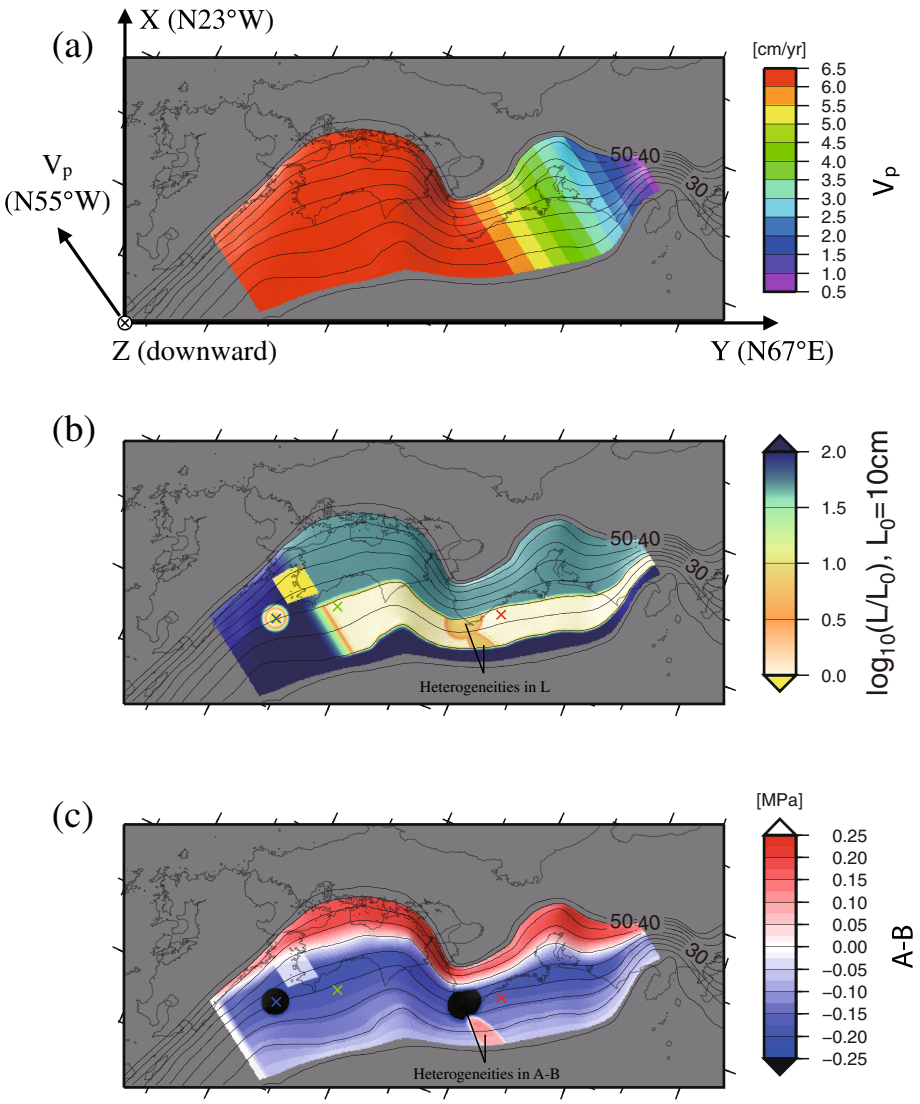

Fig. 2 Distributions of model parameters assumed in this study. **a** Assumed relative plate velocity between the Philippine Sea plate and the overlying continental plate, from Heki and Miyazaki (2001). A coordinate system for dividing the plate interface into sub-faults is also shown. **b** Characteristic slip distance, *L*. **c** *A–B*; parameter distributions from Kyushu to Kii Peninsula in (**b**) and (**c**) are from Nakata et al. (2014). Further east, depth profiles of frictional distributions at the eastern edge of the model in Nakata et al. (2014) are extrapolated to the Tokai region. Beneath and off the Kii Peninsula, heterogeneities in frictional parameters are assumed from the results of Kodaira et al. (2006) and Hori (2006). *Colored crosses* indicate positions of time series of evaluated cumulative slips in Figs. 4 and 6

from the southern tip of the Kii Peninsula to the Izu Peninsula (Fig. 2a). Such eastward decrease of back-slip rate is based on analysis of the crustal deformation velocity (Heki and Miyazaki 2001). Here, the decrease in the back-slip rate is given perpendicular to the direction of back-slip (see Fig. 2a). Note that the eastern and western edges of the model plate interface are cut along the direction of N 55° W to avoid boundary effects.

Additionally, in extending the model plate interface eastward, we incorporate the frictional heterogeneity around the Kii Peninsula (Fig. 2b, c) assumed by Kodaira et al. (2006) and Hori (2006). The heterogeneity beneath the Kii Peninsula is based on structural analyses, and it acts as the segment boundary between the Nankai and Tokai earthquakes in numerical simulations (Kodaira et al. 2006). As shown in Kodaira et al. (2006), at the segment boundary between Tokai and Nankai earthquakes, two kinds of remarkable structures are found from seismic imaging: one is a high-density and high-velocity dome body beneath Cape Shionomisaki. The other is a highly fractured oceanic crust caused by the strike slip fault system located at the shallower side of the dome structure. Kodaira et al. (2006) considered that

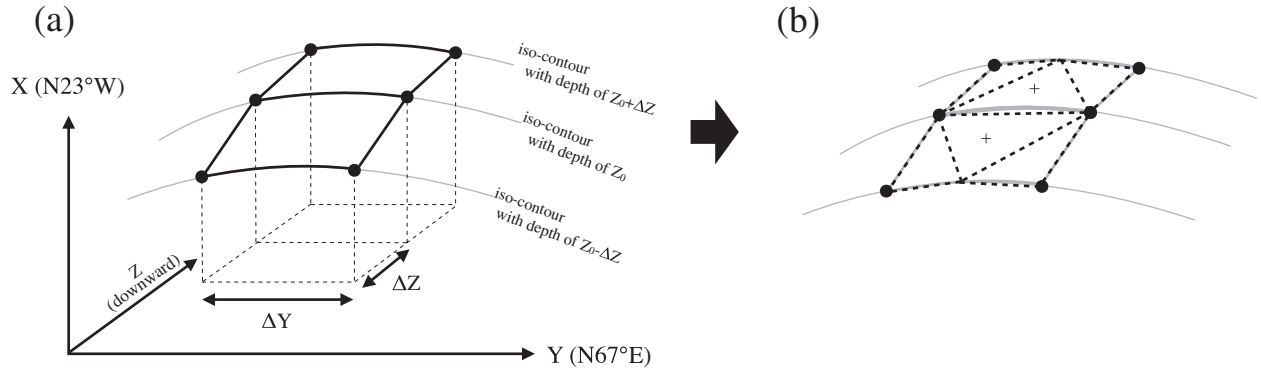

Fig. 3 Schematic illustration of the definition of sub-faults. **a** Division of the plate interface into sub-faults with non-planar shape using the projection to *Y-Z* plane of the coordinate system in Fig. 2a. **b** Approximation of a non-planar sub-fault with a set of *three triangles*

the high-density and high-velocity dome on the plate interface increases the normal stress on the plate interface and is strengthened against the rupture. Hence, in the position of the dome, they assigned large $B - A$ following the assumption of high σ, and also large L for large fracture energy. For fractured oceanic crust, they considered the fracture zone must be weak and assigned $A - B > 0$ to avoid stress accumulation. Using these ideas of Kodaira et al. (2006), in this study, we follow their model setting around the segment boundary.

To examine the effect of a Hyuga-nada earthquake on the source area of Nankai Trough earthquakes at an arbitrary time in the seismic cycle, we approximate that, just after the occurrence of the Hyuga-nada earthquake, only the fault stress on the Nankai Trough mega-thrust fault will be affected by the elastic stress release of the Hyuga-nada earthquake, because a change in the fault strength requires a time lapse or slip on the fault, based on Eq. 3. Thus, by using the elastic stress change $\Delta\tau_H(\mathrm{x})$ and no associated strength change due to a simulated M_w 7.5 Hyuga-nada earthquake (see Fig. 5f), dividing Eq. 2 for after the Hyuga-nada earthquake ($t = T_H^+$) by that for before the Hyuga-nada earthquake ($t = T_H^-$) leads to the following:

$$V\left(\mathrm{x}, T_H^+\right) = V\left(\mathrm{x}, T_H^-\right) \exp\left(\frac{\Delta\tau_H(\mathrm{x})}{A}\right), \tag{5}$$

where $V(\mathrm{x},T_H^+)$ is a modified slip velocity at x due to the occurrence of the Hyuga-nada earthquake and is accelerated (for $\Delta\tau_H > 0$) or decelerated (for $\Delta\tau_H < 0$). Accordingly, by calculating the seismic cycles with the modified velocity and pre-strength distribution as initial conditions, we can evaluate the effect of the Hyuga-nada earthquake on the basic Nankai Trough earthquake cycle for arbitrary times.

Results

When two patches in Hyuga-nada and Bungo channel are included in the Nankai seismic cycle model, Hyuga-nada earthquakes (shown by steps in the blue line in Fig. 4a) occur with shorter recurrence intervals than Nankai Trough earthquakes (shown by steps in the green and red lines in Fig. 4a). Except for the Nankai Trough earthquake around time =1310 years, large and small Nankai Trough earthquakes occur alternately. Around time =1310, we can see a small Nankai earthquake occurring only 105 years after the occurrence of a Hyuga-nada earthquake, as shown in the dashed rectangle in Fig. 4a, b. In the view of slip distributions, several years after the Hyuga-nada earthquake (Fig. 5f), a Nankai earthquake is initiated at the western edge of Shikoku Island, then propagates to the east. At the frictional heterogeneity beneath the Kii Peninsula, the rupture is arrested (Fig. 5g). After about 1 year, it propagates to the eastern part of the Kii Peninsula as a "Tokai" or "Tonankai" earthquake (Fig. 5h). As such, a Nankai earthquake occurred several years after the Hyuga-nada earthquake (M_w 7.5), it is regarded as a triggered event caused by coseismic slip or after-slip following the Hyuga-nada earthquake. However, the occurrence frequency of triggered Nankai earthquakes is too low (only several times during the 2000-year simulation) to investigate the conditions under which Nankai earthquakes are triggered by a Hyuga-nada earthquake based on observation data. Hence, we executed numerical experiments that enable us to evaluate the effect of the Hyuga-nada earthquake on the arbitrary timing of the representative Nankai Trough cycles.

We utilize Eq. 5 to evaluate the effect of the occurrence timing of an M_w 7.5 Hyuga-nada earthquake on Nankai Trough seismic cycles. Then, we explain the representative behaviors of the Nankai Trough seismic

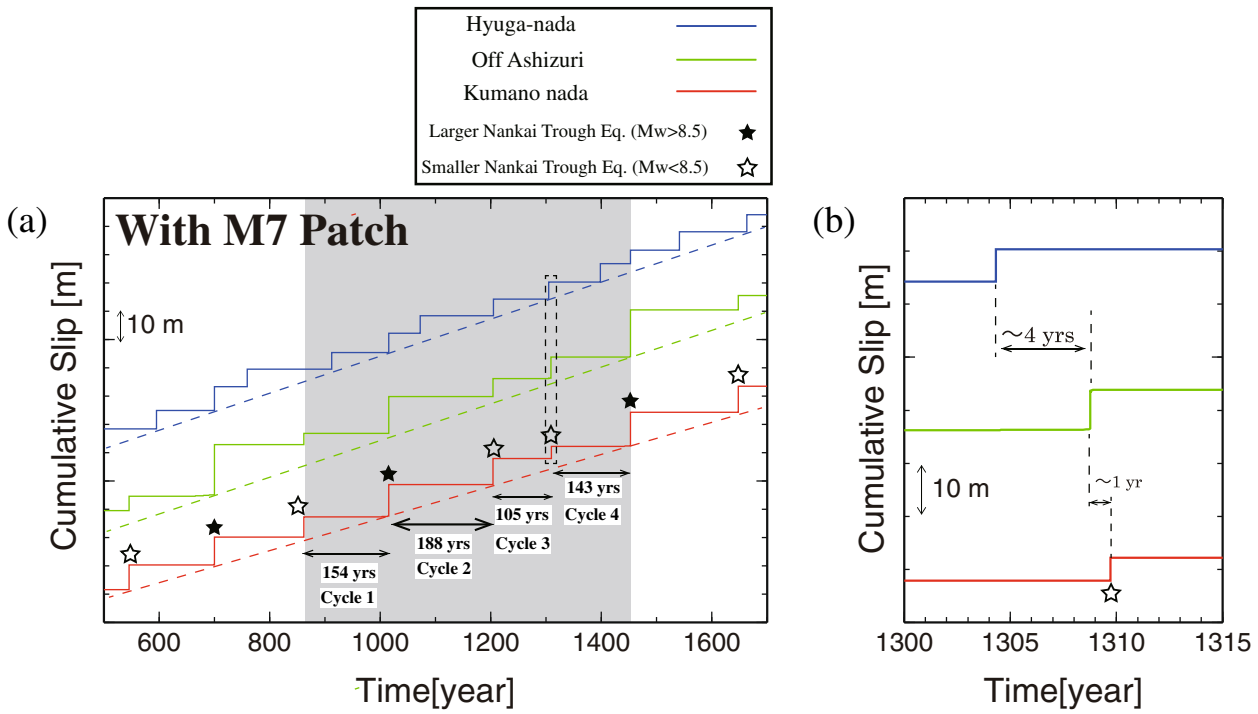

Fig. 4 a Cumulative slips in simulated Nankai Trough seismic cycles with the M_w 7 patches of Hyuga-nada and the Bungo channel. Each colored cumulative slip profile is evaluated for the cross of the same color shown in Fig. 2. *Solid* and *open stars* near the steps of the *red line* denote large ($M_w > 8.5$) and small ($M_w < 8.5$) Nankai Trough earthquakes, respectively. Except for the earthquake steps around time =1310 years, large and small Nankai Trough earthquakes occur alternately; large Nankai Trough earthquakes are accompanied by about 10 m of slip at Kumano-nada (larger steps in *red line*) and more than 10 m of slip off Ashizuri (larger steps in *green line*). Except for the small event at time =1310, small Nankai Trough earthquakes have smaller slips than the large earthquakes at both Kumano-nada and off Ashizuri, although the magnitude relationship of the slips between Kumano and Ashizuri is the reverse of that of the large earthquakes. At Hyuga-nada, more than 5 m of slip always occur with the occurrences of large earthquakes, whereas with the small earthquakes, the slips vary from 0 to about 5 m. In addition, as for the Hyuga-nada earthquakes ($M_w \sim 7.5$), several slip events at Hyuga-nada occur independently of the Nankai Trough earthquakes. **b** Close-up view of *broken rectangle* in (**a**). A Hyuga-nada earthquake triggers a Nankai earthquake, then a Tokai earthquake occurs with a time lag of 1 year

cycles by removing the M_w 7 patches in the Hyuga-nada region from the above seismic cycle model.

As shown in Fig. 6, the resultant behavior of the representative Nankai seismic cycles is as follows: two types of Nankai Trough earthquakes with large differences in magnitudes occur alternately, indicated by black ($M_w > 8.5$) and white ($M_w < 8.5$) stars in Fig. 6. As indicated in Figs. 6 and 7, the time intervals preceding the larger Nankai Trough earthquakes are shorter than those preceding the smaller earthquakes, and the variation of recurrence intervals is about 150–180 years, which is less than the variation of historical earthquakes (90–262 years). Two types of earthquakes are mainly caused by the large gap in L, or fracture energy, in the seismogenic zone, as shown in Fig. 2b, similar to Hyodo and Hori (2013). At Hyuga-nada, about 5 m of after-slips occur only after the larger Nankai Trough earthquakes. However, in the inter-seismic periods of the Nankai Trough earthquake, a regime of stable sliding is dominant (blue line in Fig. 6).

Essentially, both types of Nankai Trough earthquakes are initiated at the plate interface beneath Kumano-nada. Then, the initiated ruptures propagate eastwards and rupture the eastern segments. At the same time, westward ruptures also begin to traverse the barrier (heterogeneity shown in Figs. 2b, c) at the Kii Peninsula, crossing the barrier at different time intervals after the eastward rupture, as shown in Fig. 7. However, the rupture in the third cycle (Fig. 7f) is initiated at the western end of Shikoku and propagates eastward. This type of rupture is rarely seen, as it occurs only once in a few thousand years. As a result, there are three types of seismic cycles, depending on the size and rupture patterns.

As shown above, the behaviors of the small Nankai Trough earthquake at the end of the third cycle in Figs. 4 and 5 are representative of the triggering effect of the M_w 7.5 Hyuga-nada earthquake. To quantitatively evaluate how the triggering effect can modify the intrinsic behavior of the Nankai Trough seismic cycle, we executed numerical experiments by applying the velocity perturbation due to the M_w 7.5 earthquake shown in Eq. 5 to the three seismic cycles in Figs. 6 and 7. For evaluating Eq. 5, we adopted a slip distribution of the Hyuga-nada

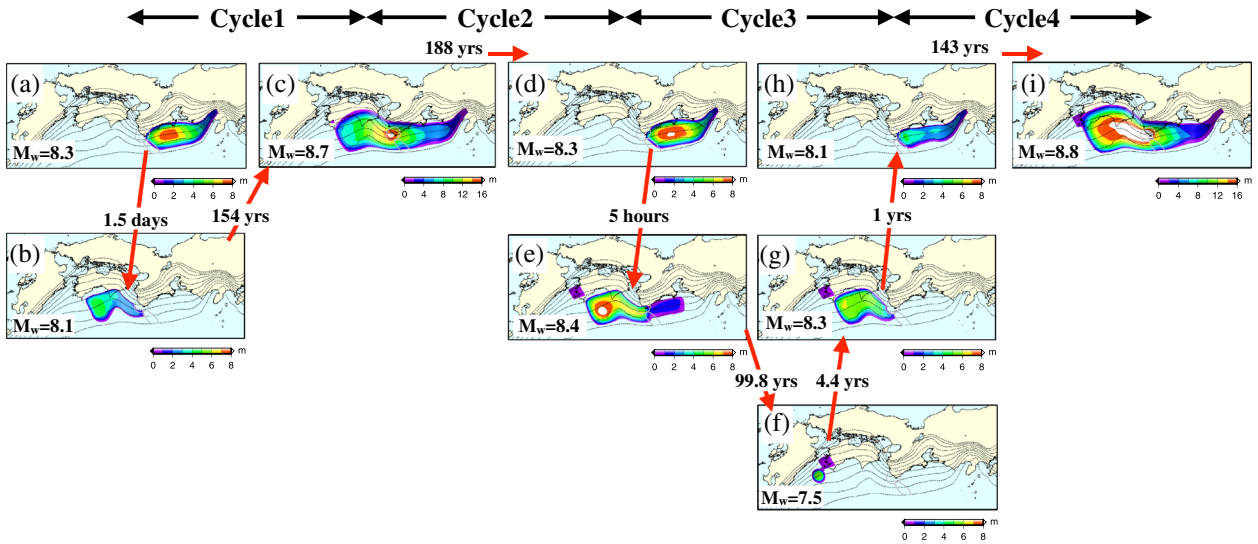

Fig. 5 Coseismic slip distributions of the Nankai Trough earthquakes and a Hyuga-nada earthquake occurred in the *shaded duration* of Fig. 4a. As shown in (**c**) and (**i**), the large Nankai Trough earthquakes break entire region from western Shikoku to Tokai region almost simultaneously. While in small earthquakes, eastern and western parts of the Nankai Trough earthquake separately occur with time lag. At the end of the third cycle (i.e., (**f**), (**g**) and (**h**)), a Nankai earthquake occurs about 5 years after the occurrence of a preceding Hyuga-nada earthquake. Then, after 1 year, the Tokai earthquake occurs separately

earthquake, as shown in Fig. 5f. Although this earthquake triggered a Nankai earthquake as shown in the above simulation, its slip distribution with maximum slip of about 6 m is not so different to other Hyuga-nada earthquakes that occurred during the interseismic periods of the Nankai Trough earthquakes (see the steps of the blue line in Fig. 4a).

The results of the numerical experiments, indicating the relationship between the trigger timing (horizontal axis) and the resultant ratio of the modified

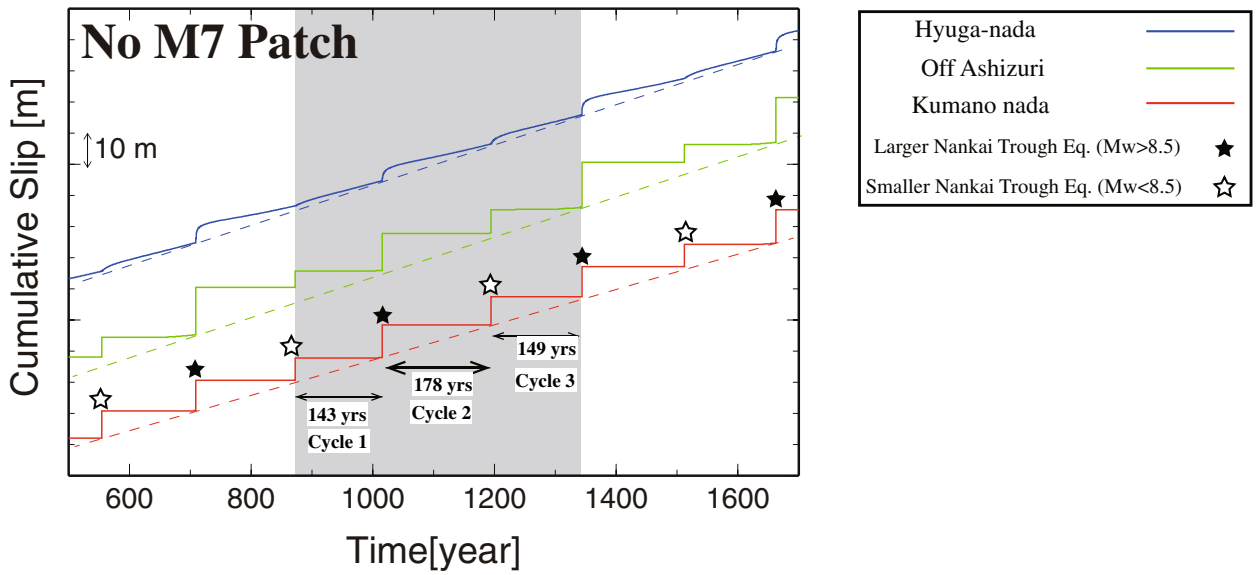

Fig. 6 Cumulative slips in simulated Nankai Trough seismic cycles without M_w 7 patches of the Hyuga-nada and Bungo channel. Each colored cumulative slip profile is evaluated at the cross with the same color as shown in Fig. 2. *Solid* and *open stars* near the steps of the *red line* denote occurrences of large ($M_w > 8.5$) and small ($M_w < 8.5$) Nankai Trough earthquakes, respectively. Large and small Nankai Trough earthquakes occur alternately; large Nankai Trough earthquakes are accompanied by about 10 m of slip at Kumano-nada (larger steps in *red line*) and more than 10 m of slip off Ashizuri (larger steps in *green line*). Small Nankai Trough earthquakes have smaller slips than large earthquakes at both Kumano-nada and off Ashizuri, although the magnitude relation of slips between Kumano and Ashizuri is opposite to the large earthquakes. At Hyuga-nada, about 5 m of after-slips occur corresponding to the occurrences of large earthquakes

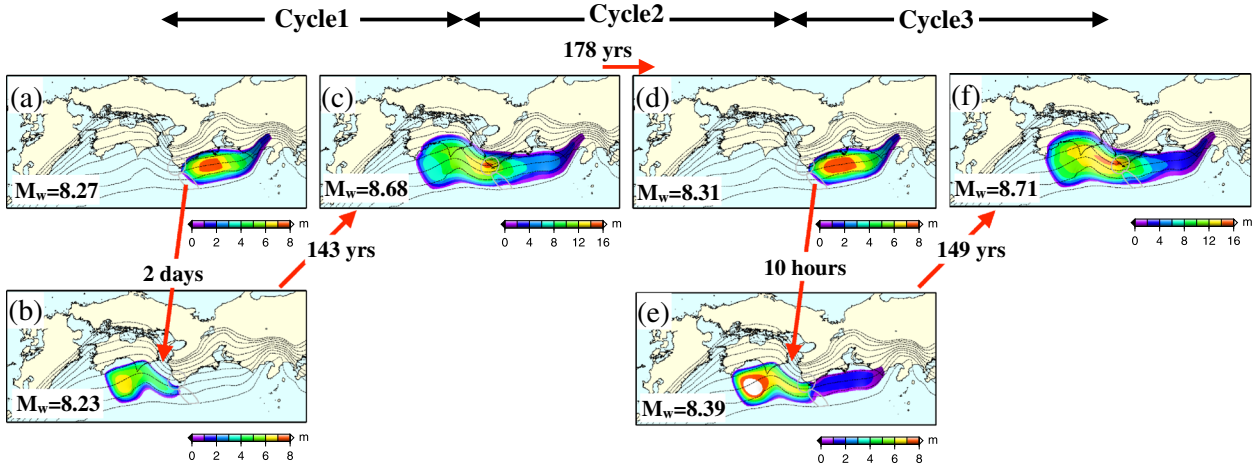

Fig. 7 Coseismic slip distributions of Nankai Trough earthquakes occurred in shaded duration of Fig. 6. Large and small Nankai Trough earthquakes occur alternately, and the interval of the seismic cycle preceding the larger Nankai Trough earthquake is shorter than that preceding the smaller earthquake. In small earthquakes at the beginning of the first cycle (i.e., (**a**) and (**b**)) and the end of the second cycle (i.e., (**d**) and (**e**)), the eastern and western segments of the Nankai Trough rupture separately with time lags of about 2 days and 10 h, respectively. In contrast, large earthquakes in (**c**) and (**f**) break the entire region from western Shikoku to the Tokai region almost simultaneously

seismic cycle to the original one (vertical axis) are shown in Fig. 8.

For cycle 1, as shown in Fig. 8a, the resultant interval of the seismic cycle varies sharply at 80 % of the time scale of the original cycle. For triggering before 80 % of cycle 1, both the rupture initiation position and timing of the next Nankai Trough earthquake are not affected, while for triggering timed after 80 %, Nankai earthquakes are initiated off Ashizuri with a delay of 3–4 years after the triggering, then the earthquake rupture propagates to the east. The maximum shortening of the seismic cycle is about 23 years, where the original interval of cycle 1 is 143 years. This is the case for the triggering at 81 % of the cycle.

Different to cycle 1, the triggered seismic cycle interval in the case of cycle 2 varies gradually (Fig. 8b), and the maximum shortening of the cycle is only 8 %, with a trigger timing of 86 %. As the original interval of cycle 2 is 178 years, the maximum shortening of the seismic cycle is about 14 years, and the interval between the trigger timing and the next Nankai Trough earthquake is about 11 years. For triggering before 60 %, rupture initiates at Kumano-nada, as shown in Fig. 7a, b, d, and e, while later triggering leads to the rupture initiation in western Shikoku.

For cycle 3 in Fig. 8c, the triggering effect varies sharply, similar to cycle 1, although the trigger timing, which minimizes the interval of the modified cycle, is much earlier than that of cycle 1: about 57 % of the original cycle for cycle 3 and 81 % for cycle 1. For triggering before 57 %, rupture initiates at Kumano-nada, but without the triggering effect, rupture initiates off Ashizuri in cycle 3. Meanwhile, for triggering after 57 %, the Nankai earthquakes are initiated off Ashizuri 2–8 years after the triggering. Among them, the maximum shortening of the seismic cycle is about 57 years for the original cycle of 149 years, corresponding to a shortening of about 40 % of the original cycle. This significant advance in time can only be seen for cycle 3. The triggered earthquakes initiated off Ashizuri tend to be arrested at the barrier beneath the Kii Peninsula, after which the eastern part of the Kii Peninsula ruptures with time lags as shown in the simulation results in Fig. 5g, h.

Many triggered earthquakes are arrested at the segment boundary at the tip of the Kii Peninsula. The time lags of triggered Nankai earthquakes for the three cycles are shown in Fig. 9, and they correlate closely with the shortening of the cycle shown in Fig. 8. The shorter the seismic cycle is truncated by the triggering, the larger the delay time between the ruptures of the eastern and western segments. On the other hand, as shown in Fig. 10, the shorter the seismic cycle, the smaller the rupture of the western segment, because the shorter recurrence time results in a smaller amount of accumulated slip deficit. Smaller rupture on the western segment results in a smaller stress concentration at the barrier beneath the Kii Peninsula (see Fig. 2b, c). This should result in a longer time to trigger rupture on the eastern segment.

Discussion

As shown in the “Results” section, during the seismic cycle following the smaller Nankai Trough earthquake, the triggered Nankai earthquake occurs in the latter half of the original recurrence interval. The eastward rupture propagation of the early triggered Nankai earthquake

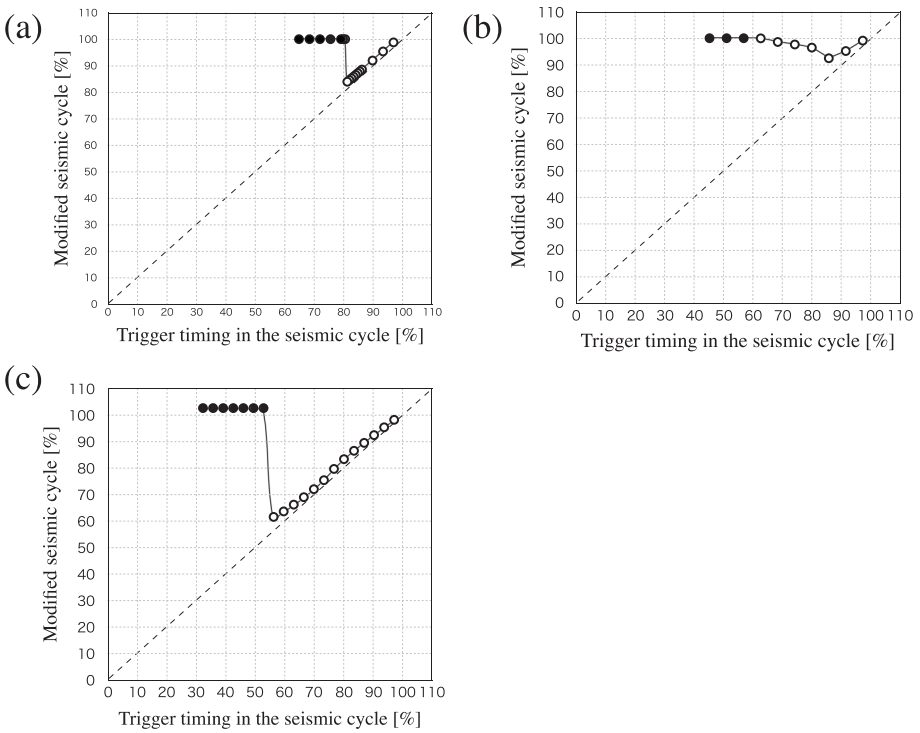

Fig. 8 Possible variations in the Nankai Trough seismic cycles due to the occurrence timing of Hyuga-nada earthquake ($M_w = 7.5$). In each panel, the *horizontal axis* indicates the given occurrence timing of the Hyuga-nada earthquake in the original seismic cycle, and the *vertical axis* is the modified seismic cycle interval with respect to the original cycle. Values less than 100 indicate shortening of the seismic cycles. **a** For cycle 1 in Fig. 6. **b** For cycle 2 in Fig. 6. **c** For cycle 3 in Fig. 6. *Open circles* indicate hypocenters of Nankai Trough earthquakes are located off Ashizuri. *Closed circles* are earthquakes with hypocenters in Kumano-nada

tends to be arrested at the barrier beneath the Kii Peninsula, and the rupture of the eastern segment occurs separately within several years after the triggered Nankai earthquake. Consequently, the magnitude of the early triggered Nankai Trough earthquake becomes small. Moreover, the early occurrence of the triggered small Nankai Trough earthquake postpones the occurrence of a larger Nankai Trough earthquake to the next seismic cycle (Fig. 11).

As shown in Figs. 8, 9, and 10, all three cycles respond quite differently to the Hyuga-nada earthquake. To consider why each cycle behaves uniquely, we focus on the time variation in the slip velocity at the initiation points of triggered Nankai Trough earthquakes. Figure 12 shows the time variation in the slip velocity for three seismic cycles in a simulation with no M_w 7 patches. The time series in Fig. 12 is evaluated offshore Ashizuri where many triggered earthquakes initiate. As shown in this figure, trigger start times at 80 and 55 % of cycles 1 and 3, respectively, correspond to a slip velocity level of around 2×10^{-3} V/V_p. On the other hand, for cycle 2, the slip velocity reaches that level just before 100 %. Since a higher slip velocity means a higher stress level relative to the strength, the velocity level is a type of threshold for triggering in our model. Although it is difficult to resolve a slip velocity on the order of 10^{-3} V/V_p from observation, the velocity reaches the order of 10^{-1} V/V_p at 85 and 70 % for cycles 1 and 3, respectively. The latter level may be resolved from observation.

From the numerical experiment results, a large advance in time of small Nankai Trough earthquakes due to a Hyuga-nada earthquake occurs only when the interplate coupling at the western part of Shikoku Island is weakened, and the slip velocity reaches a certain level, as in cycle 3 (Fig. 12). Hence, the significance of the Hyuga-nada earthquakes for the next Nankai Trough earthquake depends strongly on the current state of its earthquake cycle.

At the Bungo channel, near the Hyuga-nada region, repeated slow slip events (SSEs) have been reported since the 1990s (e.g., Hirose et al. 1999). As discussed in Nakata et al. (2014), the occurrence of SSEs may indicate the weakening of interplate coupling near the source area of the SSE. Therefore, repeated SSEs in the Bungo channel may correspond to weak coupling around the western part of the source area of the Nankai earthquake, such as in cycle 1 or 3. The estimated slip deficit rate in the SSE source area for recent decades is 0–4 cm/year, which means the slip velocity is more than 40 % of the plate convergence rate (Yoshioka et al.

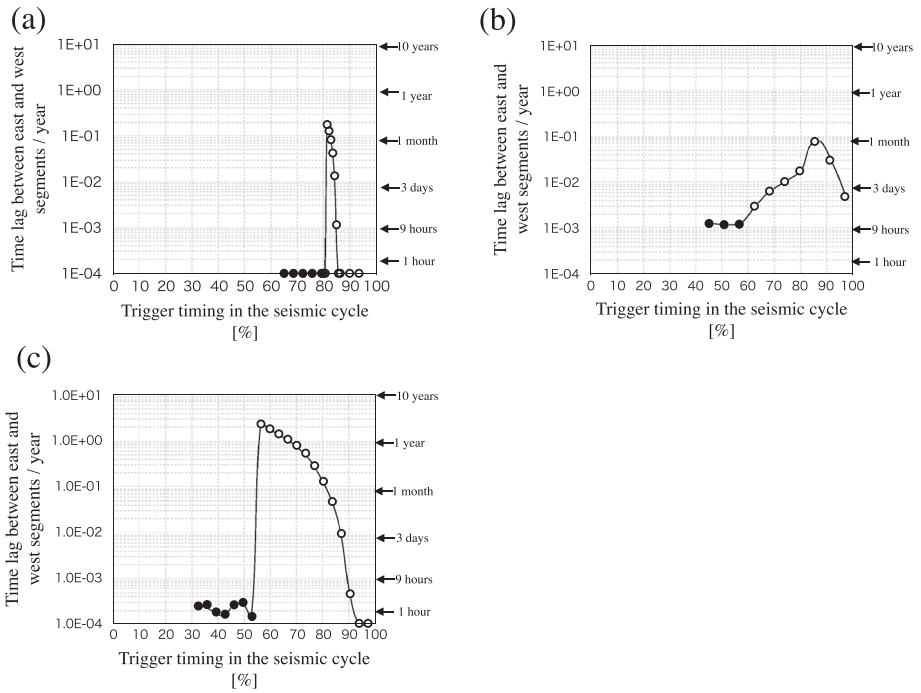

Fig. 9 Possible variations in delay of western and eastern ruptures of Nankai Trough earthquake due to the occurrence timing of Hyuga-nada earthquake ($M_w = 7.5$). In each panel, the *horizontal axis* indicates the timing of the occurrence of Hyuga-nada earthquake, and the *vertical axis* is the delay of ruptures between the western and eastern segments. **a** For cycle 1 in Fig. 6. **b** For cycle 2 in Fig. 6. **c** For cycle 3 in Fig. 6. *Open circles* indicate hypocenters of Nankai Trough earthquakes are located off Ashizuri. *Closed circles* are earthquakes with hypocenters in Kumano-nada

2015). Meanwhile, the last M_w 7 Hyuga-nada earthquake occurred in 1968, about 47 years ago. The plate convergence rate (6.5 cm/year) and the assumption of strong coupling at the source area of the Hyuga-nada earthquake lead to a slip deficit accumulation of about 3 m. In addition, after several more decades, the slip deficit on the Hyuga-nada earthquake patch will reach 4–5 m, and this amount of slip deficit will be enough to cause an M_w 7.5 earthquake.

This indicates that a triggered Nankai earthquake is likely to occur if an M_w 7 Hyuga-nada earthquake occurs. Although such a triggered Nankai earthquake was not confirmed along the Nankai Trough (i.e., the 1498 Meio earthquake is just a candidate of triggered earthquakes), it is known that several recent large earthquakes ($M_w > 8$) have occurred with foreshocks. The 2011 Tohoku earthquake (M_w 9.0) along the Japan trench occurred after 2 days of M_w 7.3 foreshock (e.g., Ando and Imanishi 2011); the 2014 Iquique earthquake (M_w 8.1) occurred within 2 weeks of foreshock activities with $M_w > 6$ (Ruiz et al. 2014). These foreshocks might trigger the following $M_w > 8$ earthquakes, as discussed in this study. Additionally, if the Hyuga-nada earthquake occurs within several decades from now, the triggered Nankai earthquake becomes immature because the elapsed time is now only about 70 years since the previous Nankai earthquake of 1946 and 1944. Thus, rupture separation between the western and eastern segments could occur for an immature and small Nankai Trough earthquake, as shown in Figs. 9c and 10c for 55–80 % trigger timing.

In contrast, if an M_w 7 Hyuga-nada earthquake does not occur in the next several decades, no matter where the next Nankai earthquake is initiated, the next Nankai Trough earthquake may be a short time interval rupture type of $M_w > 8.5$, as shown in Figs. 9c and 10c for 80–100 %.

As a current countermeasure against the next Nankai Trough earthquake, a real-time earthquake and tsunami monitoring system called dense oceanfloor network system for earthquakes and tsunamis (DONET; Kaneda et al. 2011) 1 and 2 are deployed at Kumano-nada and in the Kii channel, respectively. These areas were chosen based on a typical scenario where a Tokai (or Tonankai) earthquake initiates at Kumano-nada, then at various time intervals, a Nankai earthquake is triggered at the Kii channel, similar to the 1944 and 1946 earthquakes. However, based on the scenario proposed here, the triggered Nankai earthquake might occur before Tokai (or Tonankai) earthquake within the following several decades. Therefore, we need the real-time monitoring system to begin observations from Hyuga-nada to the western Shikoku region, the anticipated possible hypocenter location, as soon as possible. In addition, for such

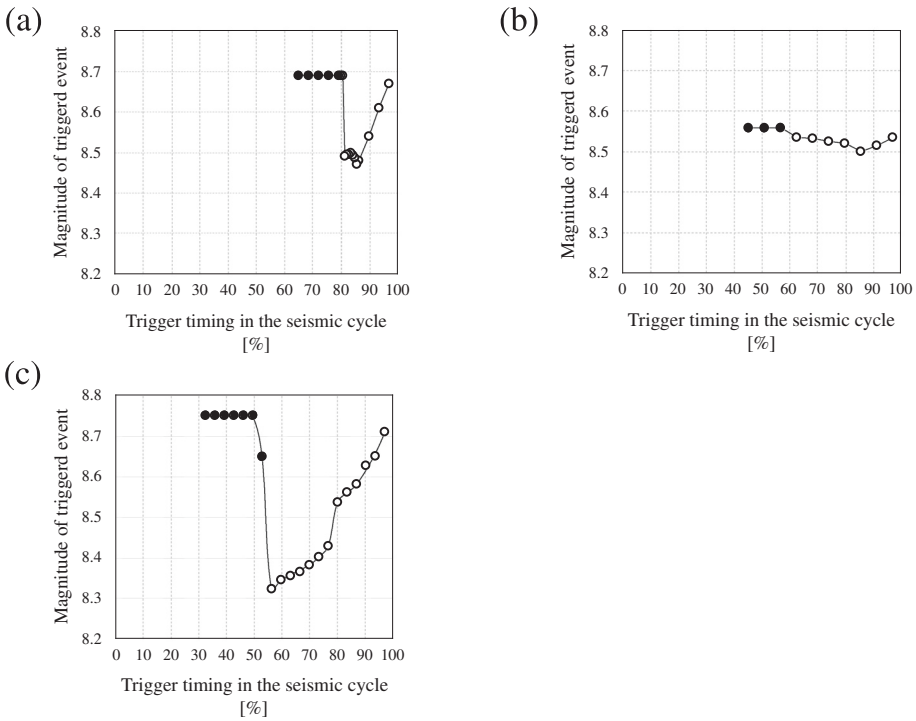

Fig. 10 Possible variations in magnitudes of Nankai Trough earthquake due to the occurrence timing of Hyuga-nada earthquake ($M_w = 7.5$). In each panel, the *horizontal axis* indicates the timing of the occurrence of Hyuga-nada earthquake, and the vertical axis is the total magnitude of ruptures in the western and eastern segments. **a** For cycle 1 in Fig. 6. **b** For cycle 2 in Fig. 6. **c** For cycle 3 in Fig. 6. *Open circles* indicate hypocenters of Nankai Trough earthquakes are located off Ashizuri. *Closed circles* are earthquakes with hypocenters in Kumano-nada

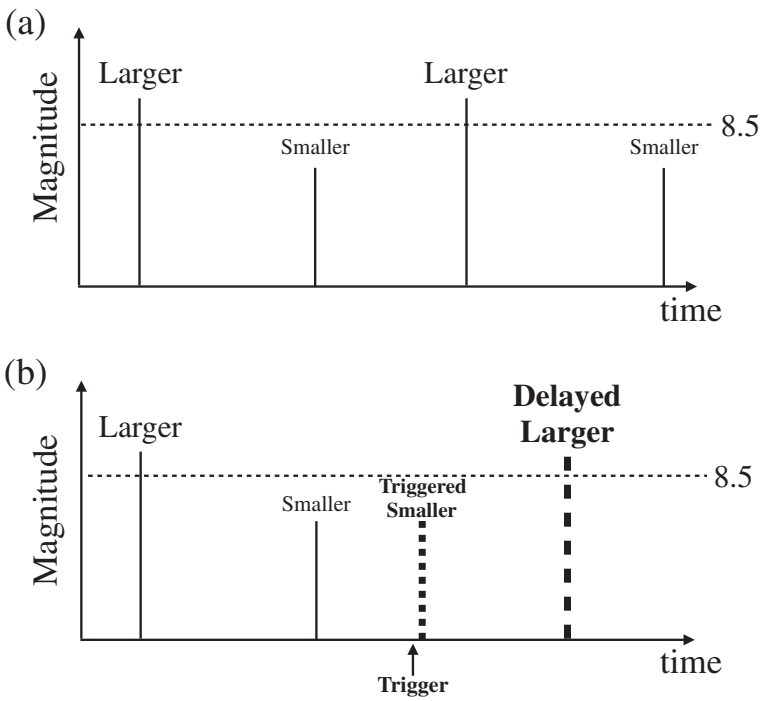

Fig. 11 Schematic illustration of seismic cycles suggested in this study. **a** Seismic cycles with nesting asperities only. **b** Possible modification of (**a**) due to triggering

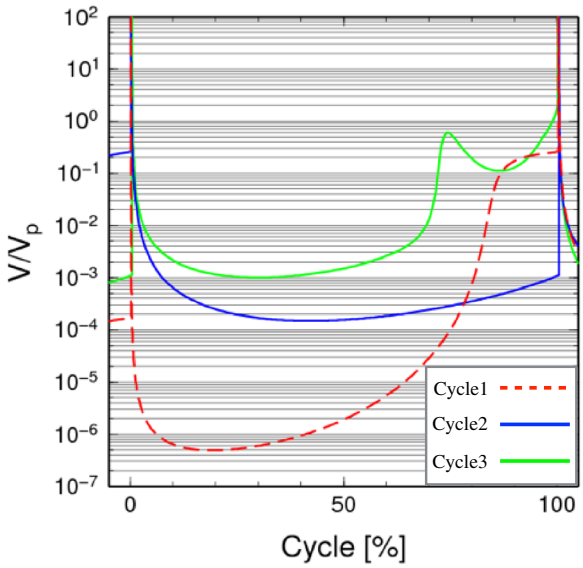

Fig. 12 Temporal variations of slip velocities during the three seismic cycles in Fig. 6 at the initiation points of simulated Nankai Trough earthquakes off Ashizuri

a scenario, detailed estimates of possible seismic and tsunami damage should be calculated, similar to those for maximum-class earthquakes.

From the numerical experiment results, the 1498 Meio Nankai Trough earthquake could be interpreted as a triggered event due to the occurrence of Hyuga-nada earthquake. In 1498, a Hyuga-nada earthquake occurred on July 9, then the Meio Tokai earthquake on the eastern Nankai Trough segments occurred after two and a half months (September 20) as shown in Fig. 1. Although the rupture timing of the western Nankai Trough segments in the Meio events has been in dispute so far, our results here suggest that a scenario which a Nankai earthquake occurred between the occurrences of the Hyuga-nada and Tokai earthquakes is physically plausible. Then, this triggered scenario for the 1498 Meio earthquake corresponds to triggered event in cycle 2 of our numerical experiments, since the preceding 1361 Ko'an Nankai Trough event was the larger one among the successive Nankai Trough earthquakes. As mentioned in the "Results" section, the minimum interval between a Hyuga-nada and triggered Nankai earthquakes is 11 years for cycle 2. The discrepancy of the simulated and 1498 trigger timings may indicate that our assumption of the Hyuga-nada earthquake with a moment magnitude of 7.5 is too small for the 1498 Hyuga-nada earthquake, because the 1498 Hyuga-nada earthquake was large enough to cause the tsunami hazards at the Chinese continent (Tsuji 1999). Since we only examined the effect of the occurrence timing of the Hyuga-nada earthquake with a fixed magnitude and location on the Nankai Trough earthquake cycles, how the variations in the magnitude or the position of the trigger earthquake affects nearby seismic cycles will be briefly considered. In our trigger model obeying Eq. 5, the sub-fault i off Ashizuri is accelerated from V_i^- to V_i^+ depending of the static stress change $\Delta\tau_{H,i}$ due to the occurrence of a Hyuga-nada earthquake. Then, during the small period Δt, slip with the amount of $U_i = V_i^+\Delta t$ is induced, and both shear stress and strength on the sub-fault i are decreased; the strength about $\sim B_iU_i/L_i$ is decreased by the slip weakening. Shear stress change on sub-fault i becomes $G_{ij}U_j$, since it is affected by slips of other sub-faults. Hereafter, we apply Einstein summation convention to only the index j. Then, according to Eq. 2, the quantity $G_{ij}U_j + B_iU_i/L_i$ represents whether the sub-fault i is accelerated (if $G_{ij}U_j + B_iU_i/L_i > 0$) or decelerated (if $G_{ij}U_j + B_iU_i/L_i < 0$) due to triggering, and it exponentially acts for the acceleration or deceleration. Our simulation results show that $G_{ij}U_j + B_iU_i/L_i$ for the sub-fault i off Ashizuri has a non-negligible positive value due to the M_w 7.5 Hyuga-nada earthquake at a later stage in cycles 1 and 3, and it grows to trigger the Nankai earthquake several years after the Hyuga-nada earthquake. Therefore, as long as the spatial distribution pattern of induced slip U_j $(1 < j < N)$ is not so different to our simulation result, Hyuga-nada earthquakes with a greater magnitude or at a closer position may dramatically shorten the time lag between a Hyuga-nada earthquake and Nankai earthquake. From this point of view, the foreshocks for the 2011 Tohoku and the 2014 Iquique earthquakes might be interpreted as triggering sources ($M_w > 6$) located close to the target earthquake. Let us consider the occurrence of a very small ($M_w << 6$) local earthquake next to the sub-fault i. Then, the local earthquake may only increase the meaningful stress on the sub-fault i. In this situation, stress change on sub-fault i will become $G_{ii}U_i$ due to the isolation of the induced slip. Then, the quality for acceleration, $G_{ii}U_i + B_iU_i/L_i$, tends to be negative, because G_{ii} is generally negative with a large absolute value. Thus, it may be hard for a single small local earthquake to accelerate nearby asperity, even if the local small earthquake generates the same stress change in the next sub-fault i as that of a distant M_w 7.5 large earthquake.

In this study, we propose a possible trigger scenario in addition to the conventional occurrence scenario in which the Nankai Trough earthquakes initiate off Kumano-nada, similar to the 1946 and 1944 events. From the numerical experiments based on the proposed scenario, in some conditions, large variations in the recurrence intervals and magnitudes of Nankai Trough earthquakes are generated owing to the triggering effect

of Hyuga-nada earthquakes. This suggests that simulations with eastern and western possible hypocenters predict more complicated seismic cycles, with larger variations of recurrence intervals and magnitudes, than those with a single hypocenter at Kumano-nada. Therefore, for more consistent reproduction of the historical Nankai Trough earthquake sequence, we should also allow several variations of hypocenter locations on the eastern segments. A seismic cycle modeling of the Parkfield segment of San Andreas Fault shows that spontaneous complexity in rupture dynamics can naturally give rise to variability in hypocenter location (Barbot et al. 2012). Though this is based on the fully elastodynamic modeling of seismic cycles, similar variability might be introduced in our quasi-dynamic model of Nankai Trough based on the more complex distribution of frictional parameters near Kumano-nada.

Seno (2012) pointed out that, based on reconsideration of the historical earthquakes, there are two possible rupture patterns on the eastern segments: the "Ansei"-type earthquake, which ruptures the D and E segments in Fig. 1, and the "Hoei"-type earthquake, which ruptures the C and D segments. Each type of earthquake has a recurrence interval of 350–400 years, and the two types of earthquakes have occurred alternately. Although the hypocenters are not explicitly mentioned in Seno (2012), since the 1944 Tonankai earthquake is categorized in Hoei-type, the hypocenters should be located on segment C in Kumano-nada. Meanwhile, for Ansei-type earthquakes, the hypocenters must be located on segment D in Enshu-nada or segment E in Suruga Bay. Hence, for the purpose of a more quantitative representation of the historical Nankai Trough earthquake sequence, applying the hypothesis of alternative hypocenters on the eastern segments to the quasi-dynamic seismic cycle simulations, which have modeled only the hypocenters in Kumano-nada, is an urgent task.

Concluding remarks

To explore possible scenarios for the next Nankai Trough earthquake, we focused on Nankai earthquakes triggered by a preceding Hyuga-nada earthquake and investigated the conditions in which such triggering occurs. As shown by the results of detailed numerical experiments, after the occurrence of smaller Nankai Trough earthquakes such as the 1946 and 1944 earthquakes, the outer extensions of the ruptured area are stressed and slide with a higher slip velocity than after the larger Nankai Trough earthquakes. Therefore, a Hyuga-nada earthquake (M_w 7.5) on the western extension of the western edge of a smaller Nankai Trough earthquake tends to trigger the occurrence of a Nankai earthquake, especially in the latter half of the seismic cycle after the smaller Nankai Trough earthquake. Hence, if a Hyuga-nada earthquake occurs within several decades from now, a Nankai earthquake may be triggered. Then, rupture separation between the western and eastern segments may also occur. Although a triggered Nankai Trough earthquake may be immature and small ($8 < M_w < 8.5$) relative to the larger class of Nankai Trough earthquakes ($M_w > 8.5$), revisions of current countermeasures against the next Nankai Trough earthquake should be performed as soon as possible. In contrast, if an M_w 7 Hyuga-nada earthquake does not occur in the next several decades, no matter where the next Nankai earthquake is initiated, it may be a large ($M_w > 8.5$), short time-interval rupture type of earthquake.

Competing interests

The authors declare that they have no competing interests.

Authors' contributions

MH processed simulated seismic cycle simulations and drafted the manuscript. TH participated in the design of the study and drafted the manuscript. YK participated in the design of the study. All authors read and approved the final manuscript.

Acknowledgements

We thank Sylvain Barbot and an anonymous reviewer for their useful comments and suggestions. The Generic Mapping Tools (GMT) package (Wessel and Smith 1995) was used to produce some of the figures. Some of the results were obtained using the K computer at the RIKEN Advanced Institute for Computational Science (Proposal number hp150215).

Author details

[1]Research and Development Center for Earthquake and Tsunami, Japan Agency for Marine-Earth Science and Technology, Yokohama 236-0001, Japan. [2]Disaster Mitigation Research Center, Nagoya University, Nagoya 464-8601, Japan.

Received: 29 September 2015 Accepted: 7 January 2016
Published online: 19 January 2016

References

Ando R, Imanishi K (2011) Possibility of M_w 9.0 main shock triggered by diffusional propagation of after-slip from M_w 7.3 foreshock. Earth Planets Space 63:767–771

Ariyoshi K, Matsuzawa T, Ampuero JP, Nakata R, Hori T, Kaneda Y, Hasegawa A (2012) Migration process of very low-frequency events based on a chain-reaction model and its application to the detection of preseismic slip for megathrust earthquakes. Earth Planets Space 64(8):693–702. doi:10.5047/eps.2010.09.003

Ariyoshi K, Matsuzawa T, Hino R, Hasegawa A, Hori T, Nakata R, Kaneda Y (2014) A trial derivation of seismic plate coupling by focusing on the activity of shallow slow earthquakes. Earth Planets Space 66(55). doi:10.1186/1880-5981-66-55

Baba T, Tanioka Y, Cummins PR, Uhira K (2002) The slip distribution of the 1946 Nankai earthquakes estimated from tsunami inversion using a new plate model. Phys Earth Planet Inter 132:59–73. doi:10.1016/S0031-9201(02)00044-4

Barbot S, Lapusta N, Avouac J (2012) Under the hood of the earthquake machine: toward predictive modeling of the seismic cycle. Science 336:707–710. doi:10.1126/science.1218796

Blanpied ML, Tullis TE, Weeks JD (1998) Effects of slip, slip rate, and shear heating on the friction of granite. J Geophys Res 103:489–511

Cabinet Office (2012) Anticipated damages due to the Nankai Trough mega-thrust earthquake (second report). http://www.bousai.go.jp/jishin/nankai/taisaku/pdf/1_1.pdf. Accessed Jan. 13, 2016

Dieterich JH (1979) Modeling of rock friction 1. Experimental results and constitutive law. J Geophys Res 84:2161–2168

Headquarters for Earthquake Research Promotion (2001) Evaluation of occurrence potentials for subduction-zone earthquakes. Nankai Trough.

Headquarters for Earthquake Research Promotion (2013) Evaluation of occurrence potentials for subduction-zone earthquakes. Nankai Trough. rev.2.

Heki K, Miyazaki S (2001) Plate convergence and long-term crustal deformation in central Japan. Geophys Res Lett 28(12):2313–2316. doi:10.1029/2000GL012537
Hirose F, Maeda K (2013) Simulation of recurring earthquakes along the Nankai trough and their relationship to the Tokai long-term slow slip events taking into account the effect of locally elevated pore pressure and subducting ridges. J Geophys Res 118:4127–4144. doi:10.1002/jgrb.50287
Hirose H, Hirahara K, Kimata F, Fujii N, Miyazaki S (1999) A slow thrust slip event following the two 1996 Hyuganada earthquakes beneath the Bungo Channel, southwest Japan. Geophys Res Lett 26(21):3237–3240. doi:10.1029/1999GL010999
Hok S, Fukuyama E, Hashimoto C (2011) Dynamic rupture scenarios of anticipated Nankai-Tonankai earthquakes, southwest Japan. J Geophys Res 116. doi:10.1029/2011JB008492.
Hori T (2006) Mechanisms of separation of rupture area and variation in time interval and size of great earthquakes along the Nankai Trough, southwest Japan. J Earth Simul 5:8–19
Hori T, Kato N, Hirahara K, Baba T, Kaneda Y (2004) A numerical simulation of earthquake cycles along the Nankai Trough in southwest Japan: lateral variation in frictional property due to slab geometry controls the nucleation position. Earth Planet Sci Lett 228:215–226
Hori T, Miyazaki S, Mitsui N (2009) A model of earthquake-generation cycle with scale-dependent frictional property—preliminary results and research plan for a project of evaluation for coming Tokai, Tonankai, and Nankai earthquakes. J Disaster Res 2:111–117
Hyodo M, Hori T (2013) Re-examination of possible great interplate earthquake scenarios in the Nankai Trough, southwest Japan, based on recent findings and numerical simulations. Tectonophysics 600:175–186
Ishibashi K (2004) Status of historical seismology in Japan. Ann Geophys 47:339–368
Kanamori H (1972) Tectonic implications of the 1944 Tonankai and the 1946 Nankaido earthquake. Phys Earth Planet Inter 5:129–139
Kaneda Y, Kawaguchi K, Araki E, Matsumoto H, Yokobiki T, Nakamura T, Kamiya S, Ariyoshi K, Baba T, Ohori M, Takahashi N (2011) Advanced ocean floor network system for megathrust earthquakes and tsunamis—DONET and DONET2 projects around the Nankai Trough. AOGS Asia Oceania Geosciences Society, Taipei, 8–12 Aug 2011
Kato N (2008) Numerical simulation of recurrence of asperity rupture in the Sanriku region, northeastern Japan. J Geophys Res 133:B06302, 10.1029/2007JB005515
Kato N, Tullis TE (2001) A composite rate- and state-dependent law for rock friction. Geophys Res Lett 28:1103–1106
Kato N, Yoshida S (2011) A shallow strong patch model for the 2011 great Tohoku-oki earthquake: A numerical simulation. Geophys Res Lett 38:L00G04. doi:10.1029/2011GL048565
Kodaira S, Hori T, Ito A, Miura S, Fujie G, Pack JO, Baba T, Sakaguchi H, Kaneda Y (2006) A cause of rupture segmentation and synchronization in the Nankai Trough revealed by seismic imaging and numerical simulation. J Geophys Res 111:B09301. doi:10.1029/2005JB004030
Matsuzawa T, Hirose H, Shibazaki B, Obara K (2010) Modeling short- and long-term slow slip events in the seismic cycles of large subduction earthquakes. J Geophys Res 115:B12301, 10.1029/2010JB007566
Nakata R, Hyodo M, Hori T (2014) Possible slip history scenarios for the Hyuga-nada region and Bungo channel and their relation with Nankai earthquakes in southwest Japan based on numerical simulations. J Geophys Res 119:4787–4801
Noda H, Lapusta N (2013) Stable creeping fault segments can become destructive as a result of dynamic weakening. Nature 493:518–521. doi:10.1038/nature11703
Ohtani M, Hirahara K, Takahashi Y, Hori T, Hyodo M, Nakashima H, Iwashita T (2011) Fast computation of quasi-dynamic earthquake cycles simulation with hierarchical matrices. Proc Com Sci 4:1456–1465
Ohtani M, Hirahara K, Hori T, Hyodo M (2014) Observed change in plate coupling close to the rupture initiation area before the occurrence of the 2011 Tohoku earthquake: implications from an earthquake cycle model. Geophys Res Lett 41:1899–1906. doi:10.1002/2013GL058751
Press WH, Teukolsky SA, Vetterling WT, Flannery BP (1996) Numerical recipes in Fortran 77: the art of scientific computing, 2nd edn. University Press, Cambridge
Rice JR (1993) Spatio-temporal complexity of slip on a fault. J Geophys Res 98:9885–9907
Ruina AL (1983) Slip instability and state variable friction laws. J Geophys Res 88:10359–10370
Ruiz S, Metois M, Fuenzalida A, Ruiz J, Leyton F, Grandin R, Vigny C, Madriaga R, Campos J (2014) Intense foreshocks and a slow slip event preceded the 2014 Iquique M_w 8.1 earthquake. Science 345(6201):1165–1169. doi:10.1126/science.1256074
Sangawa A (2009) A study of paleoearthquakes at archeological sites: a new interdisciplinary are between paleoseismology and archeology. Synthesiology (English edition) 2(2):84–94
Sangawa A (2011) Japanese history through earthquakes: what does the land tell us? Augmented edition (in Japanese). Chuokoron-shinsha, Tokyo
Seno T (2012) Great earthquakes along the Nankai Trough—a new idea for their rupture mode and time series—(in Japanese with English abstract). Zisin 64(2):97–116
Shibazaki B, Bu S, Matsuzawa T, Hirose H (2010) Modeling the activity of short-term slow slip events along deep subduction interfaces beneath Shikoku, southwest Japan. J Geophys Res 115:B00A19, 10.1029/2008JB006057
Shibazaki B, Matsuzawa T, Tsutsumi A, Ujiie K, Hasegawa A, Ito Y (2011) 3D modeling of the cycle of a great Tohoku-oki earthquake, considering frictional behavior at low to high slip velocities. Geophys Res Lett 38:L21305. doi:10.1029/2011GL049308
Shimazaki K, Nakata T (1980) Time-predictable recurrence model for large earthquake. Bulletin of the Seismological Society of America 68:279–282.
Shishikura M, Maemoku H, Echigo T, Namegaya Y, Nagai A (2011) History of multi segment earthquake along the Nankai Trough, deduced from tsunami boulders and emerged sessile assemblage. Japan Geoscience Union Meeting 2011. Makuhari Messe international conference hall, Chiba, 22–27 May 2011
Tsuji Y (1999) Nankai earthquake and its tsunami (in Japanese). Monthly Chikyu 24:36–49
Tullis TE, Salmon J, Kato N, Warren M (1999) The application of fast multipole methods to increase the efficiency of a single fault numerical earthquake model. AGU Fall Meeting Suppl 80:F924
Yoshioka S, Matsuoka Y, Ide S (2015) Spatiotemporal slip distributions of three long-term slow slip events beneath the Bungo channel, southwest Japan, inferred from inversion analyses of GPS data. Geophys J Int 201:1437–1455